



# Parametric models averaging for optimized non-parametric fragility curve estimation based on intensity measure data clustering

Konstantinos Trevelopoulos, Cyril Feau, Irmela Zentner

## ► To cite this version:

Konstantinos Trevelopoulos, Cyril Feau, Irmela Zentner. Parametric models averaging for optimized non-parametric fragility curve estimation based on intensity measure data clustering. Structural Safety, 2019, 81, pp.101865. 10.1016/j.strusafe.2019.05.002 . hal-03484490

**HAL Id: hal-03484490**

**<https://hal.science/hal-03484490>**

Submitted on 20 Dec 2021

**HAL** is a multi-disciplinary open access archive for the deposit and dissemination of scientific research documents, whether they are published or not. The documents may come from teaching and research institutions in France or abroad, or from public or private research centers.

L'archive ouverte pluridisciplinaire **HAL**, est destinée au dépôt et à la diffusion de documents scientifiques de niveau recherche, publiés ou non, émanant des établissements d'enseignement et de recherche français ou étrangers, des laboratoires publics ou privés.



Distributed under a Creative Commons Attribution - NonCommercial 4.0 International License

# **Parametric models averaging for optimized non-parametric fragility curve estimation based on intensity measure data clustering**

Konstantinos Trevelopoulos<sup>a1</sup>, Cyril Feau<sup>a</sup>, Irmela Zentner<sup>b,c</sup>

<sup>a</sup>DEN - Service d'études mécaniques et thermiques (SEMT), CEA, Université Paris-Saclay, F-91191 Gif-sur-Yvette, France

<sup>b</sup>EDF R&D, EDF Lab Paris-Saclay, 7 Bvd Gaspard Monge, 91120 Palaiseau, France

<sup>c</sup>IMSIA, UMR CNRS-EDF-CEA-ENSTA ParisTech, Université Paris-Saclay, France

## **ABSTRACT**

Seismic fragility curves give the probability of exceedance of the threshold of a damage state of a structure, or a non-structural component, conditioned on the intensity measure of the seismic motion. Typically, fragility curves are constructed parametrically assuming a lognormal shape. In some cases, which cannot be identified a priori, differences may be observed between non-parametric fragility curves, evaluated empirically based on a large number of seismic response analyses, and their estimations via the lognormal assumption. Here, we present an optimized Monte Carlo procedure for derivation of non-parametric fragility curves. This procedure uses clustering of the intensity measure data to construct the non-parametric curve and parametric models averaging for optimized assessment. In simplified case studies presented here as illustrative applications, the developed procedure leads to a fragility curve with reduced bias compared to the lognormal curve and to reduced confidence intervals compared to an un-optimized Monte Carlo-based approach. In the studied cases, this procedure proved to be efficient providing reasonable estimations even with as few as 100 seismic response analyses.

---

<sup>1</sup>Present address: French Alternative Energies and Atomic Energy Commission (CEA), DEN, 13108 Saint-Paul-lez-Durance CEDEX, France

**Keywords:** Seismic fragility curve; Non-parametric curve; Optimization; Data Clustering; Parametric Models Averaging

## 1 INTRODUCTION

A multitude of procedures is now available for probabilistic seismic assessment of structures [1]. Most notable is the framework by Yang et al. [2], which was the basis for the FEMA P-58 guidelines [3]. Here, we focus on fragility curves giving the probability to exceed a damage state threshold conditioned on a measure of the intensity of the seismic motion, such as the fragility curves defined in [4]. Such fragility curves are used for probabilistic assessment of seismic risk [5] for structures and non-structural components in nuclear installations [6] and critical civil infrastructure, such as hospitals and ports of major urban areas in earthquake prone regions [7]. They can also be used to evaluate the impact of construction details on the structural performance of installations under seismic excitations [8–11] and in rapid response applications for risk management during a seismic crisis [12]. The use of fragility curves is not limited to earthquake-related problems, they are also used in the case of other types of loading such as wind [13].

The classical formulation of a fragility curve makes the hypothesis that the curve follows a lognormal shape. D'Ayala et al. [14] and FEMA [3] describe a series of procedures for analytical fragility curve estimation, which are commonly applied. Analytical fragility curve estimation is based on Engineering Demand Parameter (EDP) observations as a function of the Intensity Measure (IM). In order to obtain such observations, either cloud analysis, Incremental Dynamic Analysis (IDA) [15] or Multiple Stripes Analysis (MSA) [16] may be performed. Linear regression [17] is a common method for lognormal fragility curve estimation. The most well established methods for adjusting a lognormal fragility curve to observations from IDA or MSA were developed by Baker [4] and are based on the method of moments and Maximum Likelihood Estimation (MLE), respectively.

However, Mai et al. [18] observed differences between non-parametric fragility curves based on kernel density estimation and lognormal fragility curves according to different procedures and highlighted the effect of the derivation procedure on lognormal fragility curves. Noh et al. [19] also used kernel smoothing in order to construct non-parametric fragility curves showing that this can be an efficient solution when using sparse data. Lallement et al. [20] consider non-parametric fragility curves more truthful representations of observations and construct curves based on generalized additive models and Gaussian kernel smoothing. Furthermore, in [21], lognormal fragility curves for structural components did not represent effectively observations from simulations of the seismic response of a bridge.

The simplest construction of a non-parametric curve puts the EDP observations in bins according to the corresponding IM and estimates empirically the probability of exceeding the damage state threshold for every bin [22]. In practice, due to the prohibitive computational cost of most nonlinear mechanical models, the development of numerically efficient methods is required to evaluate such curves using a minimal number of computations.

Here, we propose a procedure based on Monte-Carlo (MC) simulations, which uses Parametric Models Averaging (PMA) in order to optimize the computation of non-parametric fragility curves, which are constructed based on k-means clustering [23] of the intensity measure data. Optimization is employed in order to obtain reduced confidence fragility curve intervals compared to the empirical estimations with an un-optimized MC approach. The key elements of the optimization are: (i) the EDP observations are computed with seismic response analyses using synthetic accelerograms, which are realizations of stochastic processes, (ii) the non-parametric fragility curve is expressed through the law of total probability as the weighted average of parametric fragility curves, each one of which is estimated based on the synthetic ground motions generated by a stochastic process. In the optimized approach, two alternative parametric models per process are proposed for the probability of exceedance of the damage state threshold. Finally, the range of applicability of each parametric model per process is analyzed.

To illustrate the proposed methodology, “simple” stochastic processes are defined generating synthetic accelerograms based on original seed acceleration records (Section 2). The generation results in a set of synthetic accelerograms reproducing the ground motion variability observed in the original set of ground motion records. The procedure for selection of the original seed records defining the processes is out of the scope of this work. Here, for simplicity, the initial set of ground motions are selected using magnitude and distance as criteria.

Here, the non-parametric fragility curves are estimated using as IM the Peak Ground Acceleration (PGA) or the spectral acceleration at the frequency of an oscillator. However, the developed procedure is independent of the selected IM. In the studied cases, the 95 % confidence interval (CI) of the estimated fragility curves is significantly reduced due to the optimization. Moreover, the bias of the fragility curves according to the optimization is tolerable or negligible with respect to the reference curve obtained with a very large number of observations, as long as the applicability recommendations are respected.

## **2 SYNTHETIC GROUND MOTION GENERATION**

### **2.1 Motivation**

Here, synthetic ground motions are employed in order to cover the range of IMs of interest and eventually obtain fragility curves based on IM clustering that are well discretized. Moreover, synthetic ground motions are used in order to exploit the statistical characteristics of the ground motions given by a process, such as the distribution of the IMs of the generated motions, in the context of the optimization of the computation of non-parametric fragility curves. A “simple” synthetic ground motion generator is developed, which reproduces the spectral variability of recorded accelerograms, because no hypothesis is introduced concerning their frequency content. Moreover, the original recorded accelerograms are selected from the European Strong Motion Database [26,27] using simple criteria, i.e.  $5.5 < M < 6.5$  and  $R < 20$  km. Selection of the original ground motions is out of the scope of this study.

It is worth noting that the main idea in the PMA methodology is that the synthetic ground motion database consists of realizations of several stochastic processes. Therefore the methodology herein could be used theoretically in conjunction with other procedures for synthetic ground motion generation defining stochastic processes, such as the model in Rezaeian and Der Kiureghian [24]. A study of the effect of the ground motion generator is out of the scope of this article. As far as the most appropriate generator is concerned, that depends on the problem at hand and the available data (e.g. response spectra, acceleration records, see [1]).

## 2.2 Synthetic Ground Motion Generation Process

The generation process in this framework begins with retaining the FFT amplitude of every real record in the original data set, replacing the phases with a vector of uniformly distributed random values, computing the new ground motion via inverse FFT and imposing a modulation function. The result is a series of unadjusted synthetic ground motions, which are subsequently adjusted so that they are on average “spectrally equivalent” with the ground motion records in the sense of acceleration response spectra. The  $i$ -th accelerogram ( $i = \{1, \dots, N_r\}$ ) in a data set of  $N_r$  ground motion records may be expressed with Equation 1. The amplitudes ( $A_{r,im}$ ) of the  $i$ -th real record ( $\alpha_{r,i}(t)$ ) are computed with the FFT algorithm and are used in combination with random phase ( $\varphi_{s,ijm}$ ) in order to compute the  $j$ -th realization of a stationary Gaussian process (Equation 2).

$$\alpha_{r,i}(t) = \sum_{m=1}^n \left( A_{r,im} \sin(\omega_m + \varphi_{r,im}) \right) \quad i = \{1, \dots, N_r\} \quad (1)$$

$$\alpha_{s,ij}(t) = \sum_{m=1}^n \left( A_{r,im} \sin(\omega_m + \varphi_{s,ijm}) \right) \quad i = \{1, \dots, N_r\} \quad j = \{1, \dots, N_s\} \quad (2)$$

where  $\varphi_{s,ijm}$  is the phase which is assumed to be a random variable with a uniform distribution  $U(-\pi, \pi)$  according to Boore [28], and  $\omega_m$  is the  $m$ -th discrete angular frequency. The  $N_r$

stationary Gaussian processes are converted to non-stationary processes using  $N_r$  modulation functions. Here the function by Housner and Jennings [29] (Equation 3) is used, however other modulation functions, e.g. [30], may be considered.

$$q_i(t) = \begin{cases} \left(\frac{t}{T_{1,i}}\right)^3 & 0 \leq t \leq T_{1,i} \\ 1.0 & T_{1,i} < t \leq T_{2,i} \\ e^{-(t-T_{2,i})} & T_{2,i} < t \leq t_{d,i} \end{cases} \quad i = \{1, \dots, N_r\} \quad (3)$$

where  $T_{1,i}$  and  $T_{2,i}$  are the times defining the plateau of this modulation function and  $t_{d,i}$  is the total duration of the  $i$ -th acceleration record. Here,  $T_{1,i}$  and  $T_{2,i}$  are set equal to the times of observation of the 5 % and 95 % of the Arias intensity in the original acceleration record. The Arias intensity ( $I_{r,i}$ ) of the  $i$ -th acceleration record is given by Equation 4.

$$I_{r,i} = \frac{\pi}{2g} \int_0^{t_{d,i}} \alpha_{r,i}^2(t) dt \quad i = \{1, \dots, N_r\} \quad (4)$$

$T_{1,i}$  and  $T_{2,i}$  are computed with Equations 5 and 6. As an example, Figure 1a shows the modulation function used for the synthetic ground motions based on real record No. 11.

$$\frac{\pi}{2g} \int_0^{T_{1,i}} \alpha_{r,i}^2(t) dt = 0.05 \cdot I_{r,i} \quad i = \{1, \dots, N_r\} \quad (5)$$

$$\frac{\pi}{2g} \int_0^{T_{2,i}} \alpha_{r,i}^2(t) dt = 0.95 \cdot I_{r,i} \quad i = \{1, \dots, N_r\} \quad (6)$$

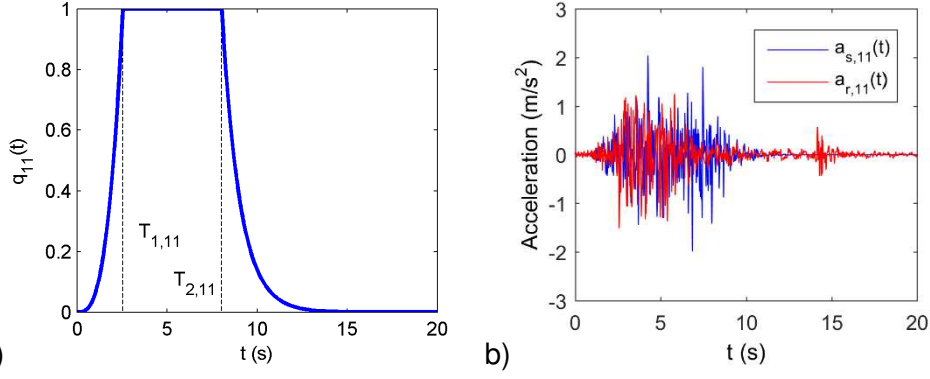


**Figure 1 a) Modulation function b) synthetic accelerogram and its original acceleration record**

The  $j$ -th realization of an unadjusted synthetic accelerogram ( $\alpha_{s0,ij}(t)$ ) based on the  $i$ -th acceleration record is given by Equation 7.

$$\alpha_{s0,ij}(t) = q_i(t) \cdot \sum_{m=1}^n \left( A_{r,im} \cdot \sin(\omega_m + \varphi_{s,ijm}) \right) \quad i = \{1, \dots, N_r\} \quad j = \{1, \dots, N_s\} \quad (7)$$

Subsequently, the synthetic ground motions generated based on an acceleration record are all scaled with the same scaling factor ( $c_i$ ), which minimizes the sum of the squares of the differences between the acceleration response spectrum of the acceleration record for 5 % damping ( $S_{a,r,i}(f)$ ) and the median spectrum for 5 % damping of the scaled synthetic ground motions ( $c \cdot \bar{S}_{a,s0,i}(f)$ ) over the frequencies between 0.2 and 25 Hz (Equation 8). The adjusted synthetic ground motions ( $\alpha_{s,ij}(t)$ ) are given by Equation 9. As an example, Figure 1b shows record No. 11 and one of its spectrally equivalent synthetic accelerograms. Figure 2 shows the acceleration response spectrum of ground motion record No. 11, the spectra of all synthetic ground motions generated based on this record and the median spectrum of the synthetics ( $c_{11} \cdot \bar{S}_{a,s0,11}(f)$ ).

$$c_i = \arg \min_{(c)} \left( \sum_{f=0.2 \text{ Hz}}^{f=25 \text{ Hz}} (S_{a,r,i}(f) - c \cdot \bar{S}_{a,s0,i}(f))^2 \right) \quad i = \{1, \dots, N_r\} \quad (8)$$



$$\alpha_{s,ij}(t) = c_i \cdot q_i(t) \cdot \sum_{m=1}^n \left( A_{r,im} \cdot \sin(\omega_m + \varphi_{s,ijm}) \right) \quad i = \{1, \dots, N_r\} \quad j = \{1, \dots, N_s\} \quad (9)$$

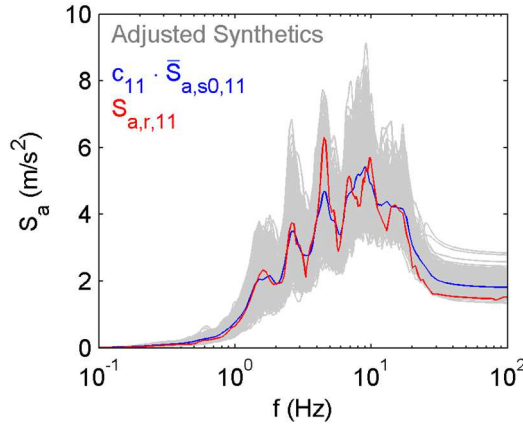


**Figure 2 Acceleration response spectra for 5 % damping of the adjusted synthetic ground motions and their original ground motion**

Based on  $N_r = 96$  original acceleration records, a total of  $N_r \times N_s = 48000$  “spectrally equivalent” synthetic accelerograms are generated ( $N_s = 500$  based on every acceleration record) in order to be used in the analytical seismic fragility curve estimation. Figure 3a shows the 15<sup>th</sup>, 50<sup>th</sup> and 85<sup>th</sup> percentiles of the acceleration response spectra for 5 % damping of the ground motion records in the data set, and the corresponding percentiles of the spectra based on the synthetic ground motions. The percentiles of the spectral values of the synthetic ground motions match well that of the acceleration records and we consider that the ground motion variability of the synthetics reproduces the variability in the original ground motion data set. We observe in Figure 3b that the percentiles of the acceleration response spectra of the synthetic ground motions for 2 % damping also match well the percentiles of the response spectra of the acceleration records. Therefore, we consider that the adjustment technique is quasi-independent of the damping value in the computation of the response spectra.

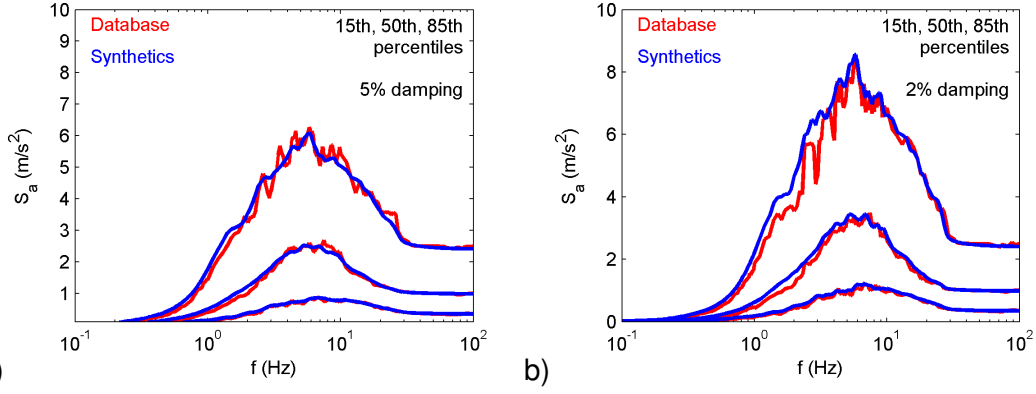


**Figure 3 Percentiles of the acceleration response spectra for a) 5 % and b) 2 % damping of the synthetic accelerograms and the ground motions in the original data set**

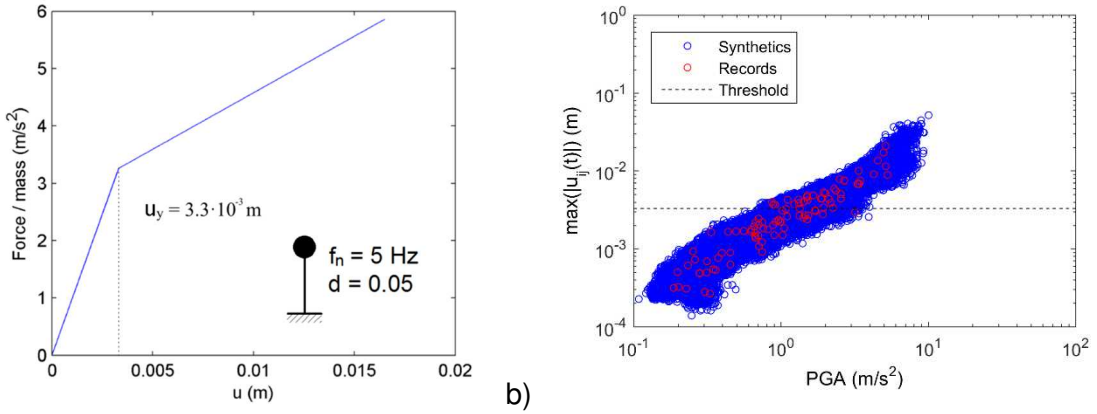
### 3 FRAGILITY CURVE CONSTRUCTION

#### 3.1 Structural Model

For the illustrative application of this framework and for verification of the PMA-based methodology an inelastic single degree of freedom structure is employed. Its frequency is 5 Hz, it has a damping ratio of 5 % and yield displacement ( $u_y$ ) of  $3.3 \cdot 10^{-3}$  m. Its post-yield stiffness, defining kinematic hardening, is equal to the 20 % of its elastic stiffness (Figure 4a). The response of the structure is computed by solving Equation 10 with the central difference method.

$$m\ddot{u}_{ij}(t) + c\dot{u}_{ij}(t) + f_{ij}(t) = -m\alpha_{s,ij}(t) \quad (10)$$

where  $m$  is the mass of the oscillator,  $\ddot{u}_{ij}(t)$  and  $\dot{u}_{ij}(t)$  are the relative acceleration and velocity of the mass, respectively, and  $f_{ij}(t)$  is the nonlinear resisting force.



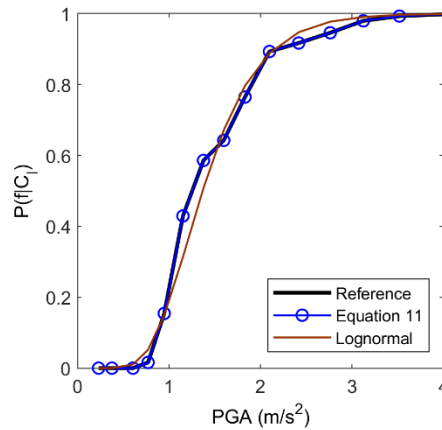
**Figure 4 a) Backbone curve of the inelastic oscillator b) maximum oscillator displacement ( $\max(|u_{ij}(t)|)$ ) observations as a function of the PGA**

Figure 4b shows the maximum response of the inelastic oscillator under excitation with the acceleration records and the generated synthetic ground motions. We observe that, in this case, the responses under the synthetic ground motions are spread over an area between and around the responses computed with the ground motion records. These data are used in the different approaches here for deriving fragility curves.

### 3.2 Empirical Non-Parametric Fragility Curves Based On MC Simulations and IM Clustering

The class of non-parametric fragility curves constructed here is based on MC simulations and clustering of the Intensity Measure observations. In the illustrative example, the maximum oscillator displacement is used as the EDP and the PGA is selected as IM for simplicity while acknowledging that other IMs may be more efficient [31]. The total Intensity Measure (IM) observations of all recorded and synthetic ground motions are classified to a number of clusters with k-means clustering [23]. K-means clustering is an iterative optimization procedure, which groups the IM observations in a selected number  $N_c$  of clusters. This procedure also returns an IM value as the centroid of each cluster. The centroid of each cluster is equal to the mean of the IM observations grouped in that cluster and the optimization procedure consists in minimizing the sum of squares of its differences from the observations

in its cluster, i.e. the variance. Here, the IM observations are grouped into  $N_c = 20$  clusters using the function “kmeans” in MATLAB [32], while the effect of IM discretization is out of the scope of this work. Subsequently, the point probabilities are classically computed at the IM cluster centroids ( $C_l, l = \{1, \dots, N_c\}$ ) as the ratio of the number of exceedances of the damage state threshold, which are observed in the analyses corresponding to the IMs in a cluster, to the number of total observations in the cluster. In this case, the damage state threshold is equal to the yield displacement ( $3.3 \cdot 10^{-3}$  m) without loss of generality. Figure 5 shows the non-parametric fragility curve computed in this case with 48096 seismic response analyses using all available recorded and synthetic accelerograms. Whenever the entirety of original and synthetic ground motions is used, the empirical Monte-Carlo-based non-parametric fragility curve will be called “reference”. The derivation of the other curves in Figure 5 follows.



**Figure 5 Lognormal, reference and fragility curve according to Equation 11**

### 3.3 New Formulation Of The Non-Parametric Fragility Curves

The proposed PMA methodology in this paper for optimized estimation of non-parametric fragility curves is based on Equation 11. This equation expresses the discrete

fragility curve  $P(f|C_l)$ , which is defined at  $N_c$  cluster centroids ( $C_l$ ), by means of the law of total probability.

$$P(f|C_l) = \frac{\sum_{i=1}^{N_r} (P(f|C_l \cap S_i) \cdot P(C_l|S_i) \cdot P(S_i))}{\sum_{i=1}^{N_r} (P(C_l|S_i) \cdot P(S_i))} \quad (11)$$

The conditional probability  $P(f|C_l \cap S_i)$  corresponds to the probability of exceeding the damage state threshold at cluster centroid  $C_l$  under excitation with ground motions originating from random process  $S_i$ . This is practically the fragility curve estimated with the ground motions originating from process  $S_i$ . The conditional probability  $P(C_l|S_i)$  is the probability of sorting the IM observations, which correspond to the ground motions belonging to process  $S_i$ , in the  $l$ -th cluster. As an example, Figures 6a and 6b show  $P(f|C_l \cap S_{23})$  and  $P(C_l|S_{23})$ , respectively, which result from an empirical computation. Finally, the probability  $P(S_i)$  equals the fraction of the number of ground motions used, which belong to random process  $S_i$ , to the total number of ground motions used to estimate the fragility curve. If we generate an equal number of synthetic ground motions for every one of  $N_r$  acceleration records, and all available ground motions are used in the computation, then  $P(S_i) = 1/N_r$ . This is the case in the validation of the Equation 11 which is presented in Figure 5. We use 96x500 synthetic ground motions generated by the random processes  $S_i$  in addition to the 96 ground motions in the original data set. Figure 5 shows that, as expected, the fragility curve defined by Equation 11 coincides with the empirical fragility curve used as reference.

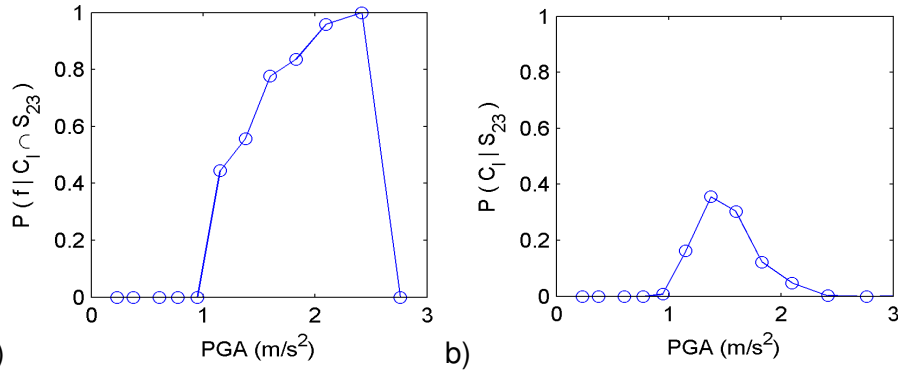


**Figure 6 a) Empirical probability of exceeding the damage state threshold ( $\max(|u_{ij}(t)|) = 3.3 \cdot 10^{-3} \text{ m}$ ) based on the synthetics generated based on the acceleration record  $S_{23}$  at the cluster centroids ( $C_i$ ) b) probability of observing a PGA value in the synthetics based on acceleration record  $S_{23}$**

### 3.4 Lognormal Curve Adjusted To The Non-Parametric Curve

In order to observe potential differences between lognormal fragility curves and the non-parametric curves estimated with the different approaches herein, a Maximum Likelihood Estimation of the lognormal cumulative distribution function is employed. The MLE of the lognormal curve uses the point probabilities constituting the empirical fragility curve based on the selected IM and corresponding EDP observations. The MLE is performed with Equations 12-15 and the estimated lognormal curve is given by Equation 16.

$$P(n_l, r_l, C_l) = \frac{n_l!}{r_l!(n_l - r_l)!} \cdot P(f|C_l)^{r_l} \cdot (1 - P(f|C_l))^{n_l - r_l} \quad (12)$$

$$L = \prod_{l=1}^{N_c} P(n_l, r_l, C_l) \quad (13)$$

$$\ln(L) = \sum_{l=1}^{N_c} \left[ \ln \left( \frac{n_l!}{r_l!(n_l - r_l)!} \right) + r_l \cdot \ln \Phi \left( \frac{\ln(C_l) - \ln(A)}{\beta} \right) + (n_l - r_l) \cdot \ln \left( 1 - \Phi \left( \frac{\ln(C_l) - \ln(A)}{\beta} \right) \right) \right] \quad (14)$$

$$\{\bar{A}, \bar{\beta}\} = \arg \max_{(A, \beta)} (\ln(L)) \quad (15)$$

$$P(f|IM) = \Phi\left(\frac{\ln IM - \ln \bar{A}}{\bar{\beta}}\right) \quad (16)$$

294

295 Where  $n_l$  is the number of EDP observations corresponding to the IM observations in the l-th  
 296 cluster,  $r_l$  is the number of EDP observations, which correspond to the IM observations in the  
 297 l-th cluster, that exceed the damage state threshold,  $C_l$  the IM centroid of the l-th cluster,  $P(f|C_l)$   
 298 the empirical fraction of EDP observations exceeding the damage state threshold in the l-th  
 299 cluster,  $P(n_l, r_l, C_l)$  the binomial distribution, L the likelihood function,  $\Phi$  the standard normal  
 300 cumulative distribution function,  $A$  and  $\beta$  the median and the dispersion of the lognormal  
 301 distribution, respectively,  $\bar{A}$  and  $\bar{\beta}$  their estimations,  $P(f|IM)$  the probability of exceeding the  
 302 damage state threshold given the IM. The difference with the curve fitting by Baker [4] is that  
 303 the fractions of damage state threshold exceedances at the cluster IM centroids are used  
 304 instead of the fractions at the IMs of EDP stripes. Figure 5 includes a lognormal curve  
 305 computed with this approach using the point probabilities, which constitute the reference  
 306 fragility curve.

#### 307 4 OPTIMIZATION WITH PARAMETRIC MODELS AVERAGING

308 In order to illustrate the optimization of the non-parametric clustering fragility curve  
 309 estimation, we are employing five approaches: (i) MC un-optimized, (ii) lognormal un-  
 310 optimized, (iii) lognormal optimized, (iv) PMA – Model 1 and PMA – Model 2, and (v) reference.  
 311 The reference curve has already been described and used in the validation of Equation 11.  
 312 PMA – Model 1 and PMA – Model 2 are the two forms of the optimized approach which are  
 313 described in Sections 4.1-4.2.

314 In the *MC un-optimized approach*, the number of seismic response analyses is firstly  
 315 selected. Subsequently, an equal number of IM observations are selected from every cluster,  
 316 equal to the number of total analyses divided by the number of clusters (rounded down to the  
 317 closest integer). If there are less IM observations in some clusters than required, we select  
 318 those available and we select the rest by selecting an even number of observations from the

rest clusters and so on. After determining the number of IM observations per cluster that will be selected, the actual selection of the IM observations is made. This selection is based on the results of k-means clustering of the IM observations based on all synthetic and recorded accelerograms. K-means returns for every IM observation the index of the cluster to which the observation is sorted. Based on the returned indices, lists of the IM observations per cluster are made and the required observations per cluster are randomly selected from the corresponding lists. Subsequently, the seismic ground motions, which correspond to the selected IM observations, are used as excitations in dynamic time-history analyses of the oscillator in order to compute EDP observations. In the MC un-optimized approach, as in the reference, the probability of exceeding the damage state threshold is estimated empirically at the  $l$ -th cluster centroid as the observed fraction of EDP observations exceeding the damage state threshold to the total number of EDP observations corresponding to the IM observations in the cluster. The lognormal curve derived using the data used in the MC un-optimized approach will be called *lognormal un-optimized*.

The optimized PMA approach is based on Equation 11 and follows the procedure of the MC un-optimized approach with three modifications. First, the conditional probability  $P(C_l/S_l)$  is not estimated with the selected IM observations, but with a very large number of IM observations in order to obtain a very precise estimation. Here, each  $P(C_l/S_l)$  distribution is empirically estimated with all available 501 IM observations; 500 observations corresponding to the synthetics and 1 to the original acceleration record. Practically, this means that the estimation of  $P(C_l/S_l)$  in the optimized approach and in the computation for the reference fragility curve are identical. It is worth noting that the estimation of  $P(C_l/S_l)$  does not require any seismic response analyses, but it requires only IM observations based on synthetic ground motions, which has a small computational cost. Second, IM observations (and the corresponding seismic ground motions used to compute EDP observations through seismic response analyses) are selected only if they are sorted in a cluster  $k_i$  where  $P(C_l/S_l)$  reaches its maximum. This is one of the key elements of the optimization process. In order to do so, the IM observations sorted in clusters other than the cluster, where  $P(C_l/S_l)$  of their process of



origin is maximized, are expunged from the lists of IM observations per cluster, from which IM observations are randomly drawn. The third and most important modification concerns the conditional probability of exceeding the damage state threshold in the case of each process ( $P(f|C_l \cap S_i)$ ). Instead of the empirical estimation of  $P(f|C_l \cap S_i)$ , the optimized approach employs two alternative parametric models. The first model (parametric model 1) assumes that  $P(f|C_l \cap S_i)$  remains constant as a function of the IM, and that it is equal to  $P(f|C_{k_l} \cap S_i)$ . The second model (parametric model 2) uses a lognormal curve for  $P(f|C_l \cap S_i)$ . In the following, the parametric models 1 and 2 are analyzed.

#### 4.1 Parametric Model 1

The first model for  $P(f|C_l \cap S_i)$  is defined by a single parameter for every process. When using this model, the optimized approach will be called *PMA – Model 1*. This one parameter is taken equal to the empirical estimation of the probability of exceeding the damage state threshold at the  $k_l$ -th IM cluster centroid, where  $P(C_l|S_i)$  obtains its maximum value (Equation 17). The one-parameter models are defined by Equation 18 and model the probability of exceeding the damage state threshold ( $P_{fi}$ ) per process as constant throughout all cluster IM centroids.

$$k_l = \underset{(l)}{\arg \max} P(C_l|S_i) \quad i = \{1, \dots, N_r = 96\} \quad l = \{1, \dots, N_c = 20\} \quad (17)$$

$$P_{fi} = P(f|C_l \cap S_i) = P(f|C_{k_l} \cap S_i) \quad i = \{1, \dots, N_r = 96\} \quad l = \{1, \dots, N_c = 20\} \quad (18)$$

As an example, Figure 7 (top left) shows the empirical conditional probability  $P(f|C_{k_{23}} \cap S_{23})$  estimated with the observations corresponding to the ground motions based on the 23<sup>rd</sup> accelerogram record. Moreover, Figure 7 (top middle) shows the corresponding model used in the optimized approach, which assumes a constant probability (red curve), which is estimated at the cluster IM centroid for which  $P(C_l|S_{23})$  is maximized (Figure 7

bottom). When employing parametric model 1, an error is introduced with respect to  $P(f|C_l \cap S_i)$ . In specific,  $P(f|C_l \cap S_i)$  is under- and overestimated at IM cluster centroids where  $C_l > C_k$  and  $C_l < C_k$ , respectively. The extent to which  $P(f|C_l \cap S_i)$  is under- or overestimated varies, and generally increases with the distance between  $C_l$  and  $C_k$ . However, the introduced error is mitigated by the fact that Equation 11 computes the product  $P(f|C_l \cap S_i) \cdot P(C_l|S_i)$ . The further  $C_l$  is found from  $C_k$ , the smallest the introduced error, because  $P(C_l|S_i)$  diminishes with the distance from  $C_k$  (e.g. Figure 7 bottom). Moreover, the fact that  $P(f|C_l \cap S_i)$  is simultaneously under- and overestimated (e.g. Figure 7 middle) at  $C_l > C_k$  and  $C_l < C_k$ , respectively, also mitigates the global error in the estimation of the fragility curve, as the underestimation on one side balances to some extent the overestimation on the other.

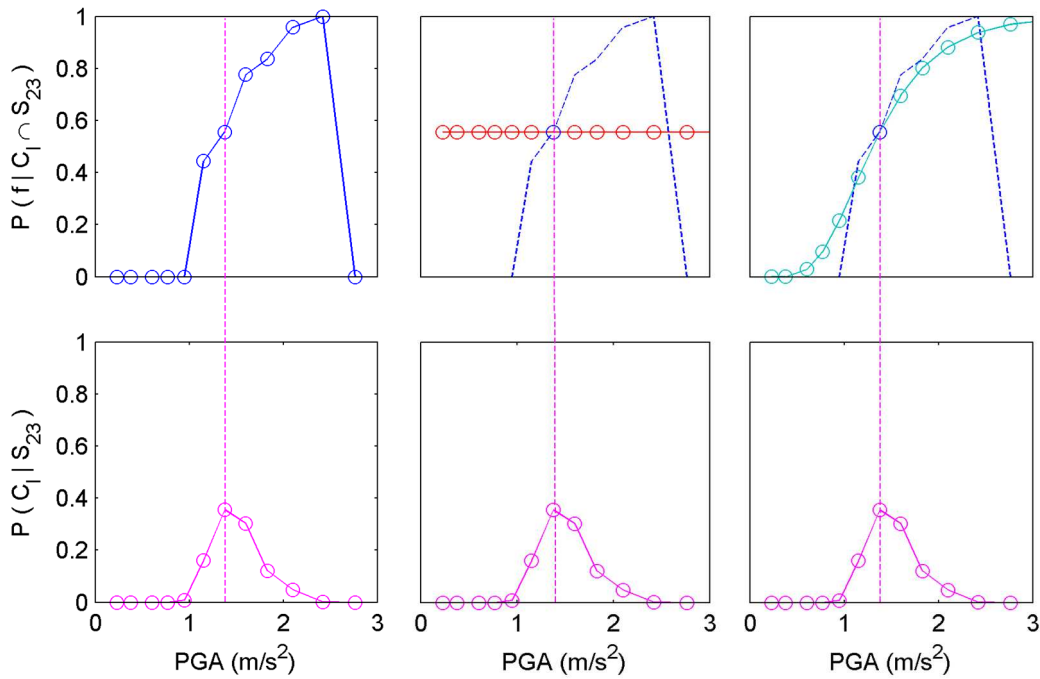


**Figure 7 Top left: Empirical fragility curve based on the ground motions originating from acceleration record 23. Top middle: parametric model 1 (constant probability of damage state threshold exceedance). Top right: parametric model 2 (lognormal model) Bottom: conditional probability  $P(C_l|S_{23})$ .**

## 4.2 Parametric Model 2

The lognormal curve is used as the second alternative parametric model for  $P(f|C_i \cap S_i)$  for every process. This form of the optimized approach will be called *PMA – Model 2*. In order to define this model for every process, two parameters are required: the dispersion and the median of the lognormal curve. These two parameters could be computed, if two or more point probabilities were available, to which the lognormal curve might be fitted. Since the optimized approach selects only IMs (and corresponding accelerograms) in cluster  $k_i$ , where  $P(C_i|S_i)$  is maximized, and computes the corresponding EDPs and  $P(f|C_{k_i} \cap S_i)$ , the only available point probability is  $(C_{k_i}, P(f|C_{k_i} \cap S_i))$ . Therefore, we assume that the dispersion of the lognormal curve for every process ( $\beta_i$ ) is equal to the dispersion of the lognormal fragility curve ( $\bar{\beta}$ , which will be referred to as  $\beta$  for simplicity), which is derived with Equations 12-16 using the data selected according to the optimized approach. This curve will be called *lognormal optimized* (there is no actual optimization here, this is simply part of the naming scheme). This allows us to compute the median of the curve for every process ( $A_i$ ) with Equation 19. Based on  $A_i$  and  $\beta_i$ , the parametric model for every process is subsequently defined with Equation 20.

$$A_i = \exp\left(\ln(C_{k_i}) - \beta_i \cdot \Phi^{-1}\left(P(f|C_{k_i} \cap S_i)\right)\right) \quad \beta_i = \beta \quad (19)$$

$$P(f|C_i \cap S_i) = \Phi\left(\frac{\ln(C_i) - \ln(A_i)}{\beta_i}\right) \quad (20)$$

As an example, Figure 7 (top right) shows  $P(f|C_i \cap S_{23})$  as estimated with the lognormal parametric model (cyan curve). In this case, the model approximates well the empirical estimation of the probability of exceeding the damage state threshold. This figure illustrates that the largest differences between the probabilities given by the model and the empirical estimation are observed where  $P(C_i|S_i)$  is close to zero. However, the empirical probabilities  $P(C_i|S_i)$  are equal to zero at the IM centroids of clusters without any IM observations.

Therefore, at such cluster IM centroids, the product  $P(f|C_i \cap S_i) \cdot P(C_i|S_i)$  in Equation 11 is always zero, which means that no error is introduced at these clusters due to the use of a parametric model for  $P(f|C_i \cap S_i)$ . As shown in the following, parametric model 2 is particularly necessary when the dispersion of the lognormal optimized fragility curve is small (approximately for  $\beta < 0.3$ ). In such cases, we consider justified to impose a common dispersion on all the parametric models corresponding to the processes  $S_i$ .

## 5 APPLICATION OF THE METHODOLOGY

In order to offer insight to the wider field of application of the developed methodology, which is essentially a MC procedure, we use it to compute the fragility curves in three cases: (i) inelastic oscillator without structural uncertainties and ground motions selected at random from the data set of all recorded and synthetic ground motions, (ii) inelastic oscillator without structural uncertainties and ground motions resulting from scaling of a single recorded accelerogram, (iii) inelastic oscillator with structural uncertainties. Based on the results of these three cases, we make our recommendations for practice. In the third case, the fragility curves are derived using as IM the PGA and the spectral acceleration at the frequency of the oscillator ( $S_a(5 \text{ Hz})$ ). To evaluate the effectiveness of the optimized procedures, we are comparing the estimated fragility curves with the reference curve and the 95 % CI according to the different approaches. The CI are computed based on bootstrap resampling [33] with a different set of 500 samples for each case.

### 5.1 Structural Model Without Uncertainties And Data Set Of Acceleration Records

The developed PMA-based optimization is firstly applied it in the case of the inelastic oscillator employed previously in the description of the methodology (Figure 4a). The ground motion data set used consists of the 96 recorded accelerograms and the 48,000 corresponding synthetic ground motions generated with the described procedure in section 2. The fragility curves are computed as a function of the PGA, for a damage state threshold

defined by a maximum oscillator displacement of  $3.3 \cdot 10^{-3}$  m, and according to the different approaches are shown in Figure 8 in the case of 100, 200, 500, and 10,000 analyses, respectively. The curves *MC un-optimized* and *lognormal un-optimized* are computed based on the same set of seismic response analyses, which is different from the set of analyses used for the optimized non-parametric curves. Every set of seismic response analyses is performed using a different and randomly selected set of ground motions according to the optimized or un-optimized approaches. Additionally, the reference non-parametric fragility curve, which is estimated based on 48096 analyses with all recorded and synthetic accelerograms, is included in the figures in order to observe any potential statistical error or bias in the evaluated curves.

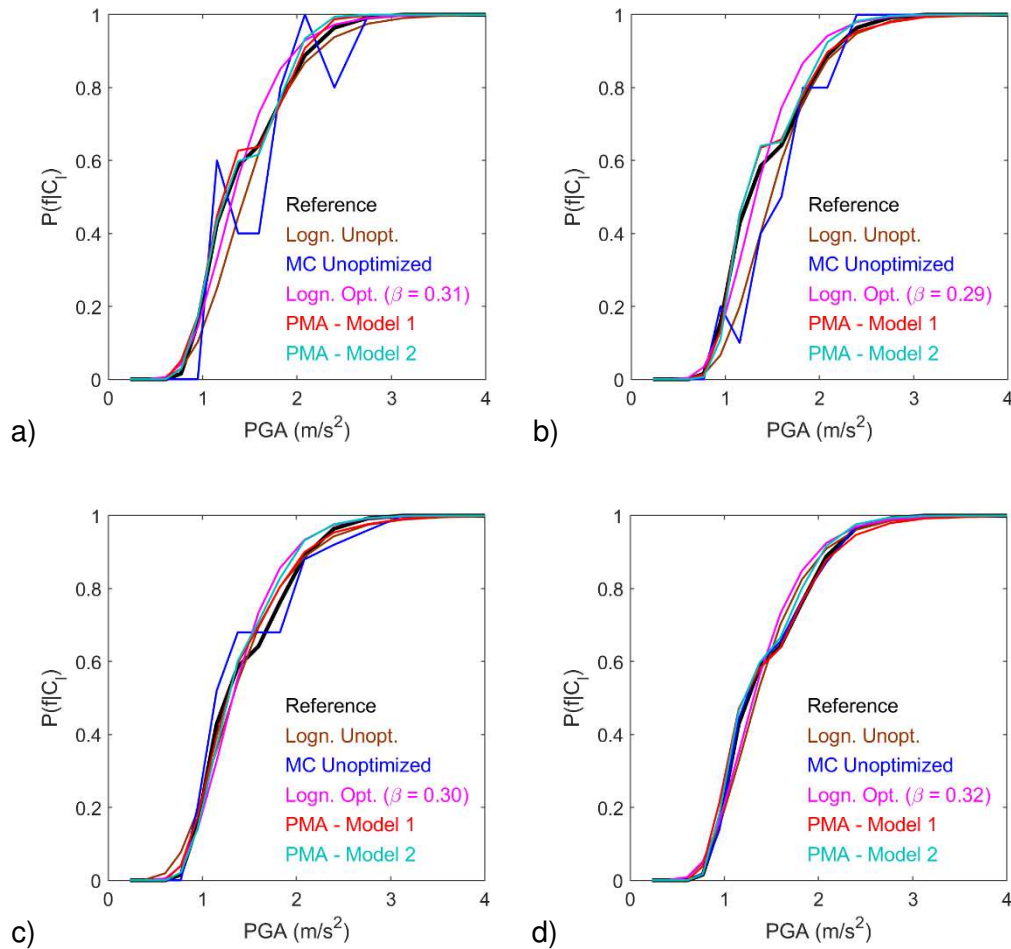


**Figure 8 Fragility curves for maximum oscillator displacement ( $\max(|u_{ij}(t)|)$ ) threshold of  $3.3 \cdot 10^{-3}$  m evaluated without structural uncertainties and with the enriched ground motion data set based all considered records and based on a) 100 b) 200 c) 500 and d) 10,000 analyses, and the reference non-parametric fragility curve**

In the case of 100, 200 and 500 seismic response analyses (Figure 8a-c), the differences between the reference and the rest fragility curves is primarily due to error of estimation. However, in the case of 10,000 analyses, the difference is rather due to a bias in the computation, given that the fragility curves are evaluated with a very large number of analyses. As far as the MC un-optimized and PMA curves are concerned, they practically converge with the reference curve as the number of analyses increases, which means that no bias is introduced due to the assumptions in this case. In Figure 8d, we observe differences between the reference and the lognormal un-optimized curve based on 10,000 analyses. Given the number of analyses, we consider that the lognormal curve is biased. More important differences between lognormal and non-parametric curves may be observed, when –among other reasons– the studied structures are more complex than a single-degree-of-freedom oscillator, as in [15]. As a measure of the estimation error, the 95 % CI of the fragility curve based on 100 analyses and according to the different approaches are shown in Figure 9. As expected, the MC un-optimized approach gives a poor estimation (Figure 9a) due to the small amount of data and the lognormal un-optimized is more effective. The CI of the curves according to the lognormal un-optimized and the PMA – Model 1 approaches appear to be equivalent (Figure 9b). However, the median lognormal un-optimized curve may converge towards a biased estimation (e.g. Figure 8). Therefore, its confidence interval is not necessarily representative of the goodness of the estimation. This is a weakness of the parametric models and it is beforehand unknown whether there is bias in the fragility curve in complex cases. We observe that the PMA – Model 1 approach results in CI which are significantly smaller than the CI according to the MC un-optimized approach (Figure 9c). According to the curves in Figure 9d, we conclude that the two forms of the PMA optimization are equally effective in this case.

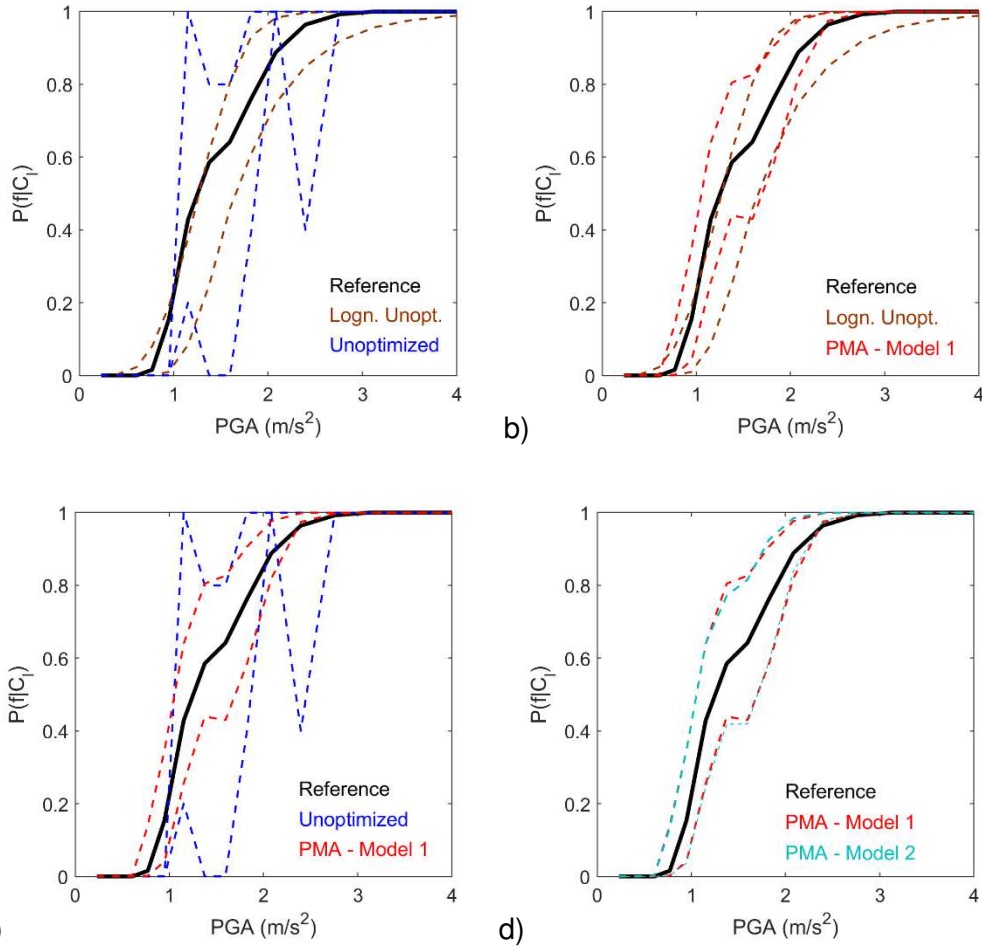


**Figure 9 95 % confidence intervals of fragility curves for maximum oscillator displacement ( $\max(|u_{ij}(t)|)$ ) threshold of  $3.3 \cdot 10^{-3}$  m evaluated without structural uncertainties and with the enriched ground motion data set based all considered records and based on 100 analyses, and the reference non-parametric fragility curve**

## 5.2 Structural Model Without Uncertainties And Data Set Of A Multiply Scaled Acceleration Record

Here we study a case with limited ground motion variability in order to demonstrate that the applicability of the developed procedures for non-parametric fragility curve estimation depends on the dispersion of the lognormal optimized curve, which is fitted to the data in an intermediate step of the computation. In this case, the synthetic ground motions are generated based on artificial accelerograms, which result from scaling multiple times (100 in this case) a randomly selected acceleration record from the 96 original real records. Based on each artificial accelerogram, 500 synthetic ground motions are generated with the procedure in

Section 2.2. Again, the oscillator in Figure 4a is employed. The maximum oscillator displacements as a function of the PGA based on all synthetic and artificial records, which are used for the reference non-parametric curve for this case, are shown in Figure 10.

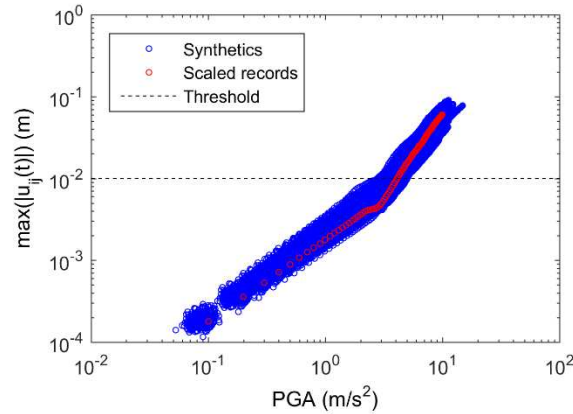


**Figure 10 Maximum oscillator displacement ( $\max(|u_{ij}(t)|)$ ) as a function of PGA computed without structural uncertainties and with the enriched ground motion data set based on scaling of a single randomly selected recorded accelerogram**

The fragility curves for a damage state threshold defined by a maximum oscillator displacement of  $1.0 \cdot 10^{-2}$  m according to the different considered approaches using 100, 200, 500, and 10,000 seismic response analyses are shown in Figure 11. In this case, all fragility curves converge to the reference with the exception of the PMA – Model 1 curve, which is based on the optimization assuming models of constant  $P(f/C \cap S_i)$  per process. It is concluded that PMA model 1 produces a biased curve contrary to PMA model 2 (Figure 11d). Nevertheless, PMA model 2 may also result in bias in other cases (not shown here), when the dispersion of the unoptimized lognormal curve is very small ( $\beta < 0.1$ ). Indeed, in such cases, the reference fragility curve tends towards a step function, which cannot be approximated by the PMA-based procedures presented here unless a finer IM discretization is considered. It should also be taken into account that the observed difference between the reference curve and the curves according to the different approaches in the case of 100 and 200 seismic response analyses is principally an estimation error due to the limited number of seismic response analyses used.



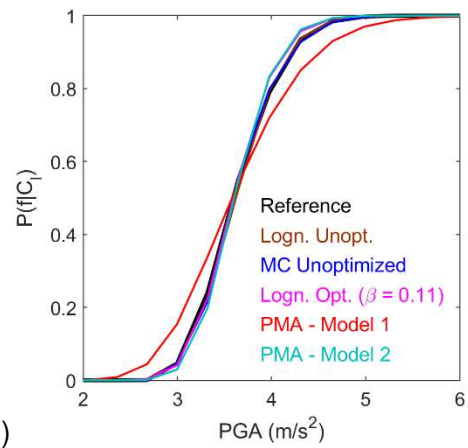
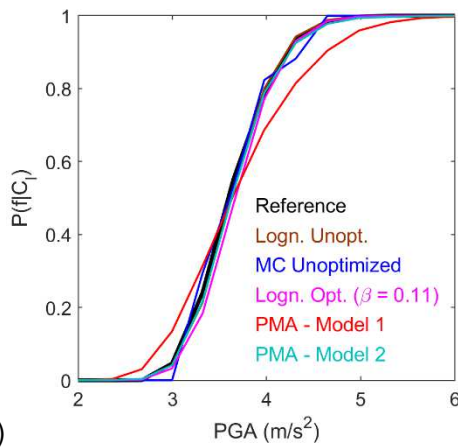
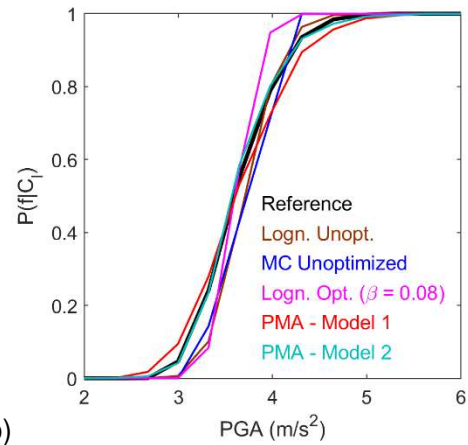
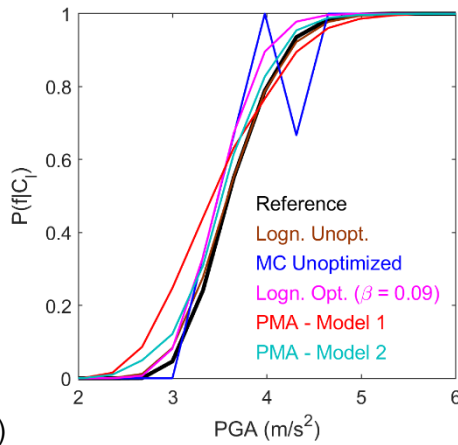


**Figure 11 Fragility curves for maximum oscillator displacement ( $\max(|u_{ij}(t)|)$ ) threshold of  $1.0 \cdot 10^{-2}$  m evaluated without structural uncertainties and with the enriched ground motion data set based on scaling of acceleration record 27 and based on a) 100 b) 200 c) 500 and d) 10,000 analyses, and the reference non-parametric fragility curve**

Figure 12 includes the 95 % CI of the fragility curves based on 100 seismic response analyses. Also in this case, the lognormal un-optimized is more effective than the MC un-optimized. The CI of the lognormal un-optimized and PMA – Model 2 curves indicate that both approaches are effective in this case, with PMA – Model 2 being slightly better. Once more, the estimation error according to the PMA – Model 2 approach is significantly less than the error in the case of the MC un-optimized computation with 100 analyses. Contrary to the CI of PMA – Model 1 curve, the CI of the PMA – model 2 curve envelopes the reference and indicates that this is the preferable approach in this case.

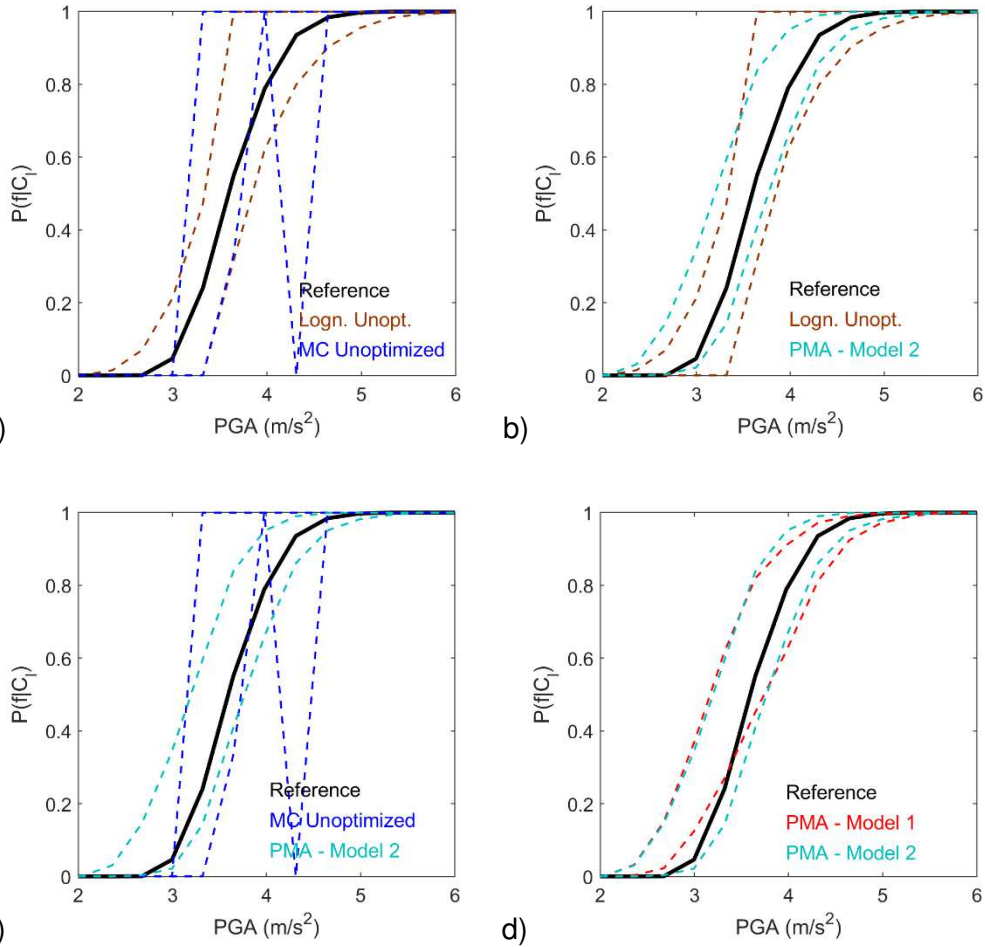


**Figure 12 95 % confidence intervals of fragility curves for maximum oscillator displacement ( $\max(|u_{ij}(t)|)$ ) threshold of  $1.0 \cdot 10^{-2}$  m evaluated without structural uncertainties and with the enriched ground motion data set based on scaling of acceleration record 27 and based on 100 analyses, and the reference non-parametric fragility curve**

### 5.3 Structural Model With Uncertainties And Data Set Of Acceleration Records

The developed optimization procedure is also applied in the case of uncertain structural parameters. In specific, the oscillator in Figure 4a is employed and uncertainty is introduced by considering the elastic frequency and the yield displacement of the oscillator as random parameters with a coefficient of variation of 0.2. To do so, in every simulation, i.e. seismic response analysis, the elastic frequency (5.0 Hz) and the yield displacement ( $3.3 \cdot 10^{-3}$  m) are multiplied with random independent values sampled from two identical normal distributions with mean and standard deviation equal to 1.0 and 0.2, respectively. Such pairs of random values are sampled with Latin Hypercube Sampling for every 96 records and 48000 synthetic

ground motions in the data set. Figure 13 shows the damage state threshold and the computed EDPs ( $\max(|u_{ij}(t)|)$ ) as a function of  $S_a(5 \text{ Hz})$  and PGA as IM, respectively.

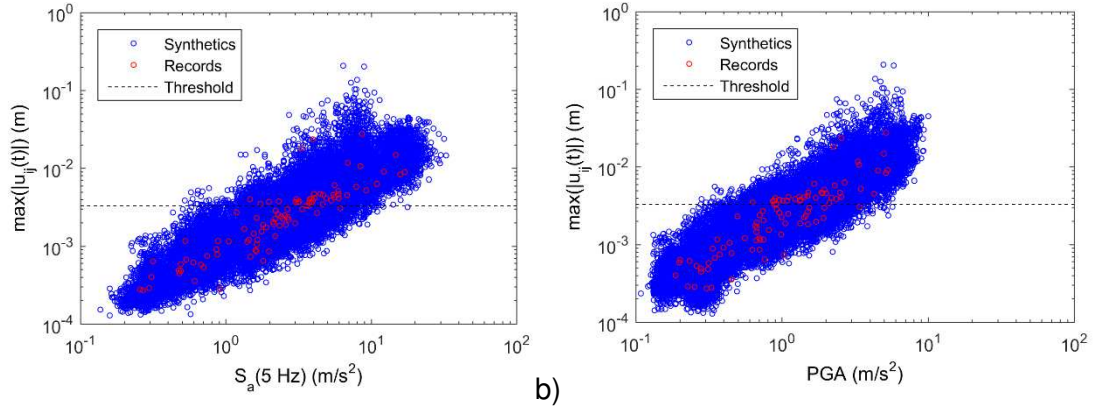


**Figure 13 Maximum oscillator displacement ( $\max(|u_{ij}(t)|)$ ) as a function of a) the spectral acceleration at 5 Hz and b) the PGA in the case of the oscillator with frequency and yield displacement uncertainty**

The fragility curves for a damage state threshold of  $3.3 \cdot 10^{-3} \text{ m}$  maximum oscillator displacement as a function of  $S_a(5 \text{ Hz})$  and PGA are shown in Figure 14 and 15. As expected, (i) the introduction of uncertainties leads to increase of the dispersion of the lognormal fragility curves and (ii) the dispersion of the lognormal fragility curves is slightly larger when PGA is considered as IM. The optimized fragility curves and un-optimized non-parametric fragility curves converge with the reference fragility curves for the two cases (Figures 14d, 15d) and present small differences from the lognormal curves. It is worth noting that the lognormal optimized curve has a dispersion of 0.48 and 0.52 when using as IM the  $S_a(5 \text{ Hz})$  and the PGA, respectively.

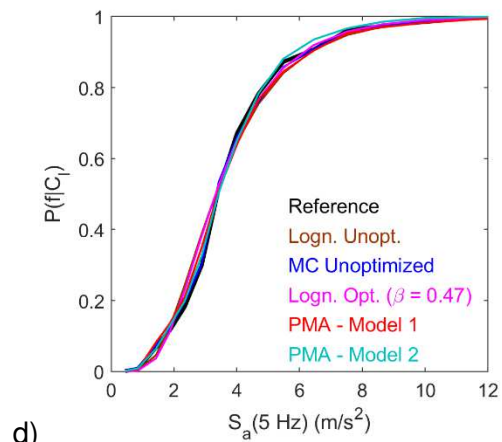
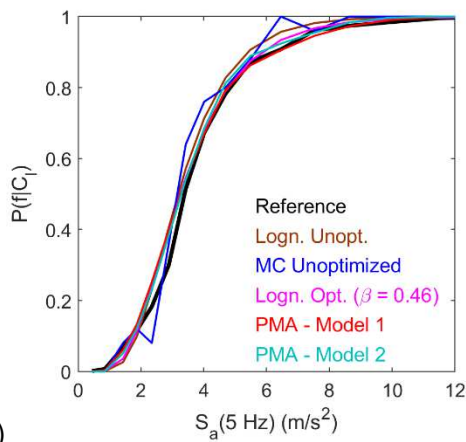
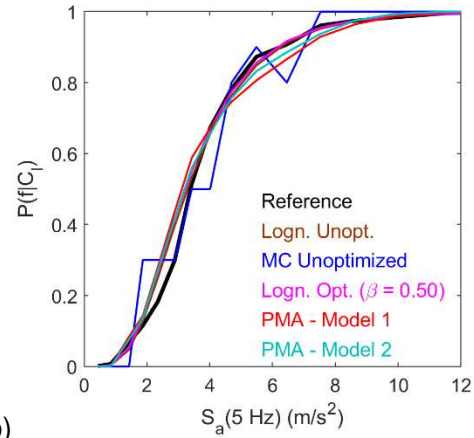
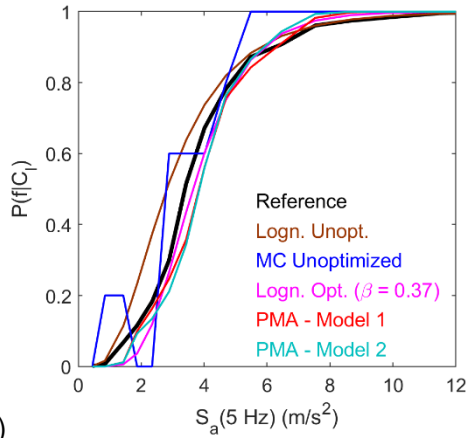


**Figure 14 Spectral acceleration ( $S_a(5\text{ Hz})$ )-based fragility curves for maximum oscillator displacement ( $\max(|u_{ij}(t)|)$ ) threshold of  $3.3 \cdot 10^{-3}\text{ m}$  evaluated with structural uncertainties and with the enriched ground motion data set based all considered records and based on a) 100 b) 200 c) 500 and d) 10,000 analyses, and the reference non-parametric fragility curve**

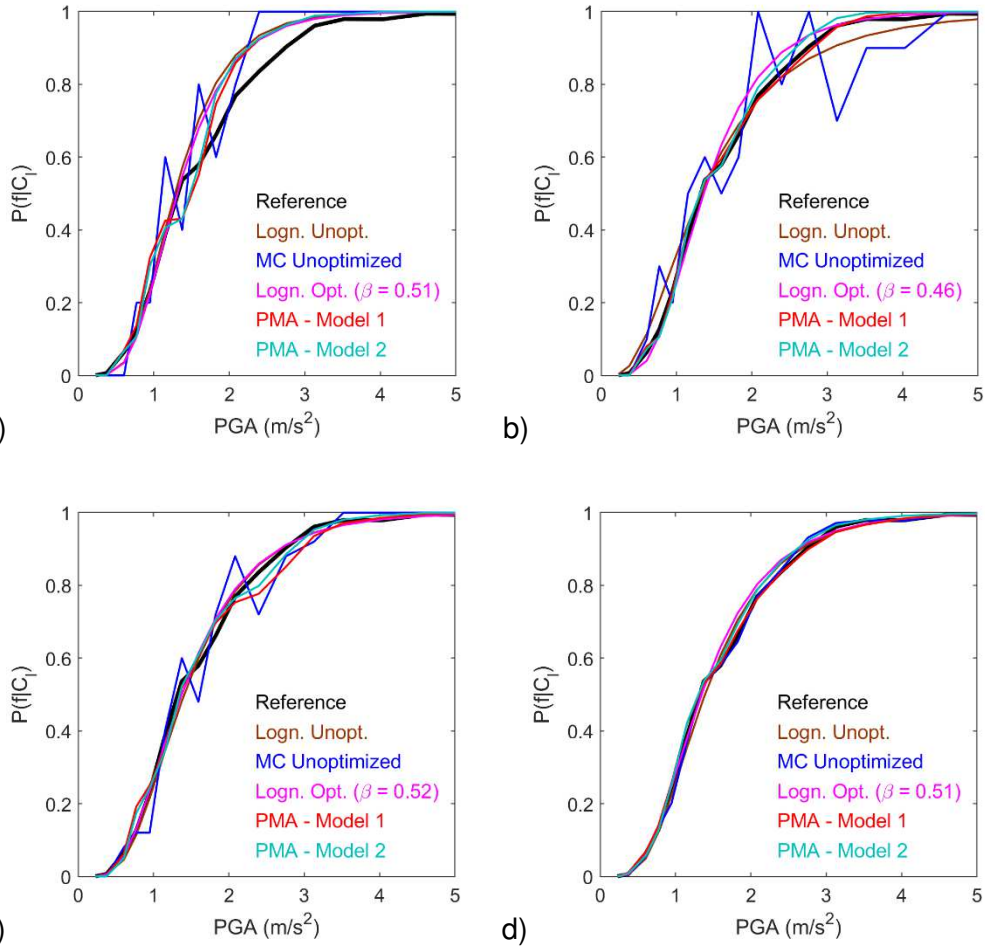


**Figure 15 PGA-based fragility curves for maximum oscillator displacement ( $\max(|u_{ij}(t)|)$ ) threshold of  $3.3 \cdot 10^{-3}$  m evaluated with structural uncertainties and with the enriched ground motion data set based all considered records and based on a) 100 b) 200 c) 500 and d) 10,000 analyses, and the reference non-parametric fragility curve**

## 6 CONCLUSION

Here, we present a procedure for optimized derivation of non-parametric fragility curves using synthetic accelerograms. The fragility curves given by the presented procedure are intended for use for a specific structure rather than for a class of structures. A simple synthetic accelerogram generator is used, which reproduces the ground motion variability observed in a data set of ground motion records. However, the presented procedure is more general since it can use synthetic ground motions from other generators as long as they define random processes similar to those defined here. Also, note that the presented procedure is

independent of the selected IM. The optimization relies on the fact that the generated synthetic signals are realizations of a series of stochastic processes, each of which is based –in this work– on an acceleration record in the original data set. Using the EDP observations based on the synthetic ground motions, a parametric fragility curve is estimated for each process. Two alternative parametric models per process are proposed: a lognormal model and a model of constant probability of exceeding the damage state threshold. Based on the estimated models for all processes considered, a non-parametric fragility curve is estimated based on PMA, which computes the weighted average of the parametric models according to the law of total probability.

For the illustrative cases herein, synthetic ground motions are generated with a “simple” generator, which uses an original set of acceleration records. The generator produces synthetic ground motions with acceleration response spectra, whose 15<sup>th</sup>, 50<sup>th</sup> and 85<sup>th</sup> percentiles match well the corresponding percentiles of the spectral values of the ground motions in the original data set. All recorded and synthetic accelerograms are used as excitations of an inelastic single degree of freedom oscillator in order to obtain EDP observations as a function of the IM and estimate a reference fragility curve. The entirety of the IM observations of the recorded and synthetic ground motions is classified to clusters with k-means clustering. The number of clusters is selected based on engineering judgment, since the effect of the number of clusters is not studied here, and may nevertheless be a factor limiting the applicability of this methodology in some cases. Subsequently, the probability of exceeding the damage state threshold is estimated empirically at the cluster IM centroids using the EDP observations corresponding to the IM observations in each cluster. The result is the MC-based empirical non-parametric fragility curve, which is used as reference, as it is considered the best estimation possible based on the IM clustering approach and the available data. In the MC un-optimized approach, the same procedure is followed, but instead of using all data, an as constant as possible number of IM observations per cluster is selected so that the total number of analyses is in accordance with the available computational time.

The PMA optimized approach builds upon the MC un-optimized estimation by introducing an additional IM observation selection criterion. The IM observations in every cluster eligible for selection are those found in clusters with maximum probability of observation given the process, which generated the corresponding synthetic ground motions. Based on the EDP observations, which correspond to the selected IM observations, the probabilities of exceeding the damage state threshold at the IM cluster centroids are empirically estimated. These probabilities are used to define the parametric fragility curve, i.e. the parametric mode, which is related to each random process. Subsequently, the parametric models are averaged with the probabilities of occurrence of each random process in the clusters which are estimated with a very large number of synthetic ground motions, with practically no computational cost, since it requires no seismic response analyses. As in [18] or [21], we observe that non-parametric curves based on the proposed procedures may present differences from lognormal curves based on the same data. Here, the smallest differences between lognormal un-optimized and non-parametric fragility curves are observed when the dispersion of the lognormal curves are either very small (e.g.  $< 0.1$ ) or considerable (e.g.  $> 0.5$ ). As far as the uncertainty of the estimated non-parametric curve is concerned, we employ non-parametric bootstrap resampling to estimate the 95 % CI of the fragility curves. Moreover, the 95 % CI of the PMA curve is reduced with respect to the CI of the MC un-optimized curve for the same number of seismic response analyses in all cases in the study. In conclusion, the developed methodology is an efficient and useful procedure for fragility curve estimation and has wider applicability than a parametric model (e.g. the lognormal), which may lead to biased estimations.

Our recommendations are summarized in Table 1. The criteria that guide us are two: the dispersion of the lognormal optimized curve fitted to the selected data and the discretization of the IM observations, i.e. the number of clusters. When applying the proposed procedure, estimating a fragility curve while using a very coarse IM discretization can be considered equivalent to the estimation of a fragility curve with a very small dispersion. In the area of 100 or less analyses, use of a typical un-optimized lognormal fragility curve is recommended. If

the resources for 10,000 or more analyses are available, the MC un-optimized approach can be used. In the area between 100 and 10,000 analyses, which is of practical interest, we suggest either a parametric curve, or a non-parametric optimized fragility curve computation with one of the two proposed alternatives. In this area, the dispersion of the optimized lognormal curve fitted to the selected data dictates the optimal approach. In the case of a large dispersion ( $0.3 \leq \beta$ ), the optimization with the constant probability of damage threshold exceedance per process is sufficient, while in the case of a limited dispersion ( $0.1 \leq \beta < 0.3$ ), the optimization with the lognormal model per process is recommended. When PMA – Model 1 and 2 use a large number of seismic response analyses and give drastically different results (as in the case with an original data set consisting of ground motions resulting from scaling a single acceleration record), PMA – Model 2 should be preferred, unless the dispersion of the associated optimized lognormal curve is very small ( $\beta < 0.1$ ). In such cases, the presented PMA approaches are not efficient and a lognormal model for the fragility curve is recommended.

**Table 1 Recommended type of fragility curve based on the number of seismic analyses (N) and the dispersion of the lognormal (un-optimized) curve fitted to the empirical non-parametric curve ( $\beta$ )**

	$\beta < 0.1$	$0.1 \leq \beta < 0.3$	$0.3 \leq \beta$
$N < 100$	Un-optimized Lognormal	Un-optimized Lognormal	Un-optimized Lognormal
$100 \leq N < 10,000$	Un-optimized Lognormal	PMA – Model 2	PMA – Model 1
$10,000 \leq N$	MC Un-optimized	MC Un-optimized	MC Un-optimized

Our procedure has also been applied in the case of a realistic finite element model of a low-rise reinforced concrete bare frame (modelling details may be found in [34]), not presented here for the sake of brevity. The results lead to the same conclusions. Should one attempt to apply the procedure herein in the case of complex structures, they will face a series of challenges, which are, however, not specific to our methodology. A major concern would be the selection of an efficient IM. IMs are considered efficient [35], when the seismic response



as a function of the IM has a low dispersion. However, scalar IMs are not efficient in every case. For example, the spectral acceleration at the first eigenfrequency is a common scalar IM, which is efficient in the case of structures, whose response is mostly affected by their first mode. However, it is not efficient in the case of tall buildings [36]. In the case of structures with multiple degrees of freedom the use of more adapted IMs, or even a vector of different IMs [37] may be a solution. That said, further investigations should be made to see if the procedures herein can be modified to use a vector IM. Although, the procedure herein is—in principle— independent of the selected IM and the damage state, it should be adapted to more severe damage states such as collapse. Indeed, the simulation of severe damage states may be computationally demanding and may require to take into account P-delta effects [38], to simulate brittle failure modes [39] and consider alternative IMs [40]. In addition, a validation of our methodology with a very large number of seismic response analyses in the case of complex structures has a prohibitive computational cost. To test the usefulness of our procedure in the case of complex structures, fragility curves given by our procedure based on a reasonable number of seismic response analyses (e.g. a few hundred) could be compared with curves given by other procedures, which reduce the computational cost. Such procedures may rely, amongst others, on metamodeling strategies based on neural networks [41], or support vector machines [42]. Finally, further studies of the developed procedure using realistic structural models and fragility curves conditioned on failure, instead of curves conditioned on an engineering demand parameter threshold, should provide additional insights.

## ACKNOWLEDGMENTS

Funding: This work was supported by the research project *SINAPS@* (ANR-11-RSNR-0022), a project of the SEISM Institute (<https://institut-seism.fr/>) funded by The French National Research Agency in the context of its program *Investments for the Future*.

## REFERENCES

- [1] Fragiadakis M, Vamvatsikos D, Karlaftis MG, Lagaros ND, Papadrakakis M. Seismic assessment of structures and lifelines. *J Sound Vib* 2015;334:29–56. doi:10.1016/j.jsv.2013.12.031.
- [2] Yang TY, Moehle J, Stojadinovic B, Der Kiureghian A. Seismic Performance Evaluation of Facilities: Methodology and Implementation. *J Struct Eng* 2009;135:1146–54. doi:10.1061/(ASCE)0733-9445(2009)135:10(1146).
- [3] FEMA. Seismic Performance Assessment of Buildings – Volume 1 – Methodology. WASHINGTON, DC: 2012.
- [4] Baker JW. Efficient Analytical Fragility Function Fitting Using Dynamic Structural Analysis. *Earthq Spectra* 2015;31:579–99. doi:10.1193/021113EQS025M.
- [5] Silva V, Crowley H, Bazzurro P. Exploring Risk-Targeted Hazard Maps for Europe. *Earthq Spectra* 2016;32:1165–86. doi:10.1193/112514EQS198M.
- [6] Berge-Thierry C, Svay A, Laurendeau A, Chartier T, Perron V, Guyonnet-Benaize C, et al. Toward an integrated seismic risk assessment for nuclear safety improving current French methodologies through the SINAPS@ research project. *Nucl Eng Des* 2017;323:185–201. doi:10.1016/j.nucengdes.2016.07.004.
- [7] Tsionis G, Mignan D, Pinto A, Giardini D, European Commission, Joint Research Centre. Harmonized approach to stress tests for critical infrastructures against natural hazards. Luxembourg: Publications Office; 2016.
- [8] Zhang J, Huo Y. Evaluating effectiveness and optimum design of isolation devices for highway bridges using the fragility function method. *Eng Struct* 2009;31:1648–60. doi:10.1016/j.engstruct.2009.02.017.
- [9] Saha SK, Matsagar V, Chakraborty S. Uncertainty quantification and seismic fragility of base-isolated liquid storage tanks using response surface models. *Probabilistic Eng Mech* 2016;43:20–35. doi:10.1016/j.probengmech.2015.10.008.

729 [10] Patil A, Jung S, Kwon O-S. Structural performance of a parked wind turbine tower  
730 subjected to strong ground motions. *Eng Struct* 2016;120:92–102.  
731 doi:10.1016/j.engstruct.2016.04.020.

732 [11] Gidaris I, Taflanidis AA, Mavroeidis GP. Kriging metamodeling in seismic risk  
733 assessment based on stochastic ground motion models: Seismic Risk Assessment Through  
734 Kriging Metamodeling. *Earthq Eng Struct Dyn* 2015;44:2377–99. doi:10.1002/eqe.2586.

735 [12] Parolai S, Haas M, Pittore M, Fleming K. Bridging the Gap Between Seismology and  
736 Engineering: Towards Real-Time Damage Assessment. In: Pitilakis K, editor. *Recent Adv.*  
737 *Earthq. Eng. Eur.*, vol. 46, Cham: Springer International Publishing; 2018, p. 253–61.  
738 doi:10.1007/978-3-319-75741-4\_10.

739 [13] Quilligan A, O'Connor A, Pakrashi V. Fragility analysis of steel and concrete wind  
740 turbine towers. *Eng Struct* 2012;36:270–82. doi:10.1016/j.engstruct.2011.12.013.

741 [14] D'Ayala D, Meslem A, Vamvatsikos D, Porter K, Rossetto T, Silva V. Guidelines for  
742 Analytical Vulnerability Assessment - Low/Mid-Rise. GEM; 2015.

743 [15] Vamvatsikos D, Cornell CA. Incremental dynamic analysis. *Earthq Eng Struct Dyn*  
744 2002;31:491–514. doi:10.1002/eqe.141.

745 [16] Jalayer F, Cornell CA. Alternative non-linear demand estimation methods for  
746 probability-based seismic assessments. *Earthq Eng Struct Dyn* 2009;38:951–72.  
747 doi:10.1002/eqe.876.

748 [17] Zentner I. A general framework for the estimation of analytical fragility functions based  
749 on multivariate probability distributions. *Struct Saf* 2017;64:54–61.  
750 doi:10.1016/j.strusafe.2016.09.003.

751 [18] Mai C, Konakli K, Sudret B. Seismic fragility curves for structures using non-parametric  
752 representations. *Front Struct Civ Eng* 2017;11:169–86. doi:10.1007/s11709-017-0385-y.

753 [19] Noh HY, Lallemand D, Kiremidjian AS. Development of empirical and analytical fragility  
754 functions using kernel smoothing methods: DEVELOPMENT OF FRAGILITY FUNCTIONS  
755 USING KERNEL SMOOTHING METHODS. *Earthq Eng Struct Dyn* 2015;44:1163–80.  
756 doi:10.1002/eqe.2505.

757 [20] Lallemand D, Kiremidjian A, Burton H. Statistical procedures for developing earthquake  
758 damage fragility curves: STATISTICAL PROCEDURES FOR DAMAGE FRAGILITY  
759 CURVES. *Earthq Eng Struct Dyn* 2015;44:1373–89. doi:10.1002/eqe.2522.

760 [21] Karamlou A, Bocchini P. Computation of bridge seismic fragility by large-scale  
761 simulation for probabilistic resilience analysis: BRIDGE SEISMIC FRAGILITY BY LARGE-  
762 SCALE SIMULATION FOR RESILIENCE. *Earthq Eng Struct Dyn* 2015;44:1959–78.  
763 doi:10.1002/eqe.2567.

764 [22] Porter K, Kennedy R, Bachman R. Creating Fragility Functions for Performance-Based  
765 Earthquake Engineering. *Earthq Spectra* 2007;23:471–89. doi:10.1193/1.2720892.

766 [23] Jain AK, Murty MN, Flynn PJ. Data clustering: a review. *ACM Comput Surv*  
767 1999;31:264–323. doi:10.1145/331499.331504.

768 [24] Rezaeian S, Der Kiureghian A. Simulation of synthetic ground motions for specified  
769 earthquake and site characteristics. *Earthq Eng Struct Dyn* 2010;n/a-n/a.  
770 doi:10.1002/eqe.997.

771 [25] Zentner I, Poirion F. Enrichment of seismic ground motion databases using Karhunen-  
772 Loève expansion. *Earthq Eng Struct Dyn* 2012;41:1945–57. doi:10.1002/eqe.2166.

773 [26] Ambraseys N, Smit P, Sigbjornsson R, Suhadolc P, Margaris B. Internet-Site for  
774 European Strong-Motion Data. European Commission, Research-Directorate General,  
775 Environment and Climate Programme; 2002.

776 [27] Ambraseys N, Smit P, Douglas J, Margaris B, Sigbjornsson R, Olafsson S, et al.  
777 Internet site for European strong-motion data. *Boll Geofis Teor E Appl* 2004;45:113–29.

778 [28] Boore DM. Simulation of Ground Motion Using the Stochastic Method. *Pure Appl*  
779 *Geophys* 2003;160:635–76. doi:10.1007/PL00012553.

780 [29] Housner G, Jennings P. Generation of Artificial Earthquakes. *J Eng Mech Div*  
781 1964;90:113–52.

782 [30] Rodolfo Saragoni G, Hart GC. Simulation of artificial earthquakes. *Earthq Eng Struct*  
783 *Dyn* 1973;2:249–67. doi:10.1002/eqe.4290020305.

784 [31] Kostinakis K, Fontara I-K, Athanatopoulou AM. Scalar Structure-Specific Ground  
785 Motion Intensity Measures for Assessing the Seismic Performance of Structures: A Review. J  
786 Earthq Eng 2018;22:630–65. doi:10.1080/13632469.2016.1264323.

787 [32] MATLAB. MathWorks; 2015.

788 [33] Iervolino I. Assessing uncertainty in estimation of seismic response for PBEE. Earthq  
789 Eng Struct Dyn 2017;46:1711–23. doi:10.1002/eqe.2883.

790 [34] Trevelopoulos K, Guéguen P. Period elongation-based framework for operative  
791 assessment of the variation of seismic vulnerability of reinforced concrete buildings during  
792 aftershock sequences. Soil Dynamics and Earthquake Engineering 2016;84:224–37.  
793 doi:10.1016/j.soildyn.2016.02.009.

794 [35] Luco N, Cornell CA. Structure-Specific Scalar Intensity Measures for Near-Source and  
795 Ordinary Earthquake Ground Motions. Earthq Spectra 2007;23:357–92.  
796 doi:10.1193/1.2723158.

797 [36] Jayaram N, Lin T, Baker JW. A Computationally Efficient Ground-Motion Selection  
798 Algorithm for Matching a Target Response Spectrum Mean and Variance. Earthq Spectra  
799 2011;27:797–815. doi:10.1193/1.3608002.

800 [37] Kohrangi M, Bazzurro P, Vamvatsikos D. Vector and Scalar IMs in Structural Response  
801 Estimation, Part II: Building Demand Assessment. Earthq Spectra 2016;32:1525–43.  
802 doi:10.1193/053115EQS081M.

803 [38] Eads L, Miranda E, Krawinkler H, Lignos DG. An efficient method for estimating the  
804 collapse risk of structures in seismic regions: AN EFFICIENT METHOD FOR ESTIMATING  
805 THE COLLAPSE RISK OF STRUCTURES. Earthq Eng Struct Dyn 2013;42:25–41.  
806 doi:10.1002/eqe.2191.

807 [39] Kyriakides NC, Pantazopoulou SJ. Collapse Fragility Curves for RC Buildings  
808 Exhibiting Brittle Failure Modes. J Struct Eng 2018;144:04017207.  
809 doi:10.1061/(ASCE)ST.1943-541X.0001920.

810 [40] Eads L, Miranda E, Lignos DG. Average spectral acceleration as an intensity measure  
811 for collapse risk assessment: Average Spectral Acceleration as an IM for Collapse Risk  
812 Assessment. *Earthq Eng Struct Dyn* 2015;44:2057–73. doi:10.1002/eqe.2575.

813 [41] Wang Z, Pedroni N, Zentner I, Zio E. Seismic fragility analysis with artificial neural  
814 networks: Application to nuclear power plant equipment. *Eng Struct* 2018;162:213–25.  
815 doi:10.1016/j.engstruct.2018.02.024.

816 [42] Saint R, Feau C, Martinez J, Garnier J. Efficient Seismic fragility curve estimation by  
817 Active Learning on Support Vector Machines (submitted). *Struct Saf* n.d.

818